Complexation of Fluorenone and Xanthone to Cyclodextrins: Comparison of Theoretical and Experimental Studies

R. S. Murphy,[†] T. C. Barros,[†] J. Barnes,[†] B. Mayer,*[,§,‡] G. Marconi,*[,⊥,||] and C. Bohne*[,†,▽]

Department of Chemistry, University of Victoria, P.O. Box 3065, Victoria, BC, Canada V8W 3V6, Institute for Theoretical Chemistry and Radiation Chemistry, University of Vienna, UZAII, Althanstrasse 14, A-1090 Vienna, Austria, and Istituto FRAE-CNR, Via Gobetti 101, 40129 Bologna, Italy

Received: May 6, 1998; In Final Form: September 11, 1998

The structural aspects for the complexation of xanthone and fluorenone to α- as well as *β*-cyclodextrins (CDxs) were explored by combining absorption, fluorescence, and induced circular dichroism studies with theoretical calculations of the optimized structures for the ketone−CDx complexes and their predicted ICD spectra. Detailed information on the similarities and differences for the complexes of these ketones with CDxs was obtained. For both CDxs, the ketones are bound to the rim of the cavity, and deeper penetration is observed for the complexes with *β*-CDx. In addition, a 1:2 complex involving α-CDx was only observed in the case of fluorenone. Although the two ketones have similar structures, their molecular recognition properties and the resulting structures of the CDx complexes show distinct differences.

Introduction

Cyclodextrins (CDxs) are cyclic oligosaccharides formed from D-glucose units that provide a relatively hydrophobic binding site for guest molecules. The most common CDxs have six (α), seven (*β*), or eight (*γ*) glucose units for which the internal cavity diameter varies between 5 to 8 Å.[1−3] CDxs have been widely employed as host molecules in supramolecular chemistry, since the size of their cavities can be systematically varied and the hydroxyl groups at both rims can be derivatized.[4] In addition, CDxs are chiral, and this property has been explored for separation technology[5] and in the study of the complexation of various guests.

Guest molecules can interact with different regions of the CDx, and different inclusion modes have been observed, e.g., inclusion within the cavity or binding to the rim. Cartoon representations frequently show an inclusion mode where the guest is located deeply within the CDx cavity, a perception that probably arises from the fact that the cavity is relatively hydrophobic. However, in an alternative mode of inclusion the guest interacts with the rim of the cavities without penetrating deeply into the CDx. NMR spectroscopy,[6−10] where the shift of the CDx protons is analyzed, and induced circular dichroism (ICD)[11−18] spectra have been instrumental in gaining experimental evidence for the guest inclusion modes. In the case of ICD, the inclusion of an achiral molecule leads to circular dichroism signals due to its interaction with the chiral environment of the CDxs. In this respect, ICD provides information on the complexed guest without interference of signals due to the guest free in aqueous solution. An additional aspect related to CDx complexation is that frequently complexes with different guest/CDx stoichiometries are formed. These different stoichiometries have to be taken into account when spectroscopic techniques, such as ICD, are employed to gain information on the structure of the CDx complex.

The sign and strength of the ICD signal of an achiral guest molecule are directly related to the distance and orientation between the transition dipole of the guest's chromophore and the nonsymmetric bonds of the CDx. A general scheme has been developed[12−14] that determines from the sign of the ICD signal if the axis of the guest is oriented along or perpendicular to the CD*x* axis. However, this scheme, which predicts the ICD sign for a guest molecule placed inside or outside a chiral and ideally truncated cone-shaped host,[12] appears oversimplified. Recent work has shown that the sign and strength of the ICD spectra can be calculated more realistically by combining the Kirkwood−Tinoco framework to a statistical optimization of the guest−CDx structures, obtained through the dynamic Monte Carlo approach.[15−18]

A number of guest molecules have been shown to form host−guest complexes with cyclodextrins,[19] and the thermodynamics of this interaction has been well established. Less is known about the complexation dynamics.[20] Knowledge of the exit/entry rate constants is important when cyclodextrins are employed as supramolecular structures to perform specific functions, such as catalysis. However, the magnitude of the entry/exit rate constants cannot be extrapolated from equilibrium constant values. Xanthone has proven to be the only guest molecule to date for which the complexation dynamics can be followed directly with a spectroscopic method,[21−23] but the exit rate constants observed are larger than those determined for other compounds such as naphthalene derivatives.[24−27] In this respect, it is important to determine the structure of the xanthone/CDx complex in order to understand how the host−guest structure affects the complexation dynamics of guest molecules. At this point there is no information available that could indicate if there is any correlation between the exit and entry rate constants and the position of the guest molecule in the cyclodextrin

* To whom correspondence should be addressed.
[†] University of Victoria.
[‡] E-mail: bernd@asterix.msp.univie.ac. Web site: http://asterix.msp.univie.ac.at/local-link.
[§] University of Vienna.
[||] E-mail: MARC@bofra3.frae.bo.cnr.it. Web site: http://bofra3.frae.bo.cnr.it/marc.
[⊥] Istituto FRAE-CNR.
[▽] Telephone: 250-721-7151. Fax: 250-721-7147. E-mail: bohne@uvic.ca. http://www.foto.chem.uvic.ca/.

10.1021/jp9821681 CCC: $18.00
Published on Web 12/11/1998

complex. NMR can in principle be employed to obtain information about the structure of the host−guest complex. However, in the case of xanthone its concentration (<50 μM) is too low to employ NMR to determine the structure of the complex. For this reason, the complexation of xanthone and fluorenone

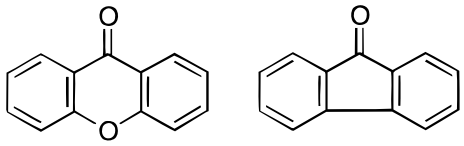

with α- and β-CDx was examined using a combined spectroscopic and theoretical approach in order to gain information about the structure of their complexes. Fluorenone was included in these studies to provide a comparison between guest molecules that are ketones and have a similar size.

Experimental Section:

Materials. 9-Fluorenone (Aldrich, 98%) and xanthone (Aldrich, 97%) were recrystallized from ethanol/water and ethanol, respectively. α-Cyclodextrin (α-CD, lot F 8035) and β-cyclodextrin (β-CD, lots C6 034-13 and F 6080-191) were a generous gift from Cerestar and were used without further purification. The water employed was deionized (SYBRON, Barnstead), whereas cyclohexane (Caledon Laboratories Ltd., spectrograde) was passed through a silica gel column (Anachemia Science, silica gel 60, 70−230 mesh) before being used. All other solvents were used as received.

Equipment. Cary 1 or Cary 5 spectrometers were employed to measure UV−vis absorption spectra at room temperature, and baseline corrections were always performed. When necessary, further corrections for the absorption of the CDx were performed by subtracting the CDx absorbance values from that measured for fluorenone or xanthone CDx complexes. When a CDx concentration dependence study was performed, the CDx spectrum was recorded for its highest concentration and the spectra at lower concentrations were calculated by taking into account the appropriate dilutions.

Induced circular dichroism (ICD) spectra were recorded with a Jasco-720 spectropolarimeter (10 nm/min and 8 s response) using a 10 mm cell. An average of two or three spectra were obtained for samples containing fluorenone or xanthone. To obtain a baseline, the circular dichroism spectrum was recorded for aqueous solutions of fluorenone or xanthone, which do not have any circular dichroism signals, since these molecules are achiral. However, by collecting the baseline with fluorenone or xanthone, the photomultiplier voltage for the baseline run in the region where these ketones absorb strongly will be similar to that for the samples containing fluorenone or xanthone and CDx. The spectra for either α- or β-CDx in water were subtracted from those containing fluorenone or xanthone in the presence of CDxs.

Steady-state fluorescence spectra were collected with a PTI QM-2 spectrofluorimeter at 20.0 ± 0.5 °C. The emission and excitation slits were set such that the bandwidths were 2 nm. The excitation wavelength used for α-CD/fluorenone samples was 300 nm, and the emission scan was recorded between 310 and 590 nm. The weak emission from impurities in the CDx samples was subtracted from the fluorescence spectra of fluorenone/CDx complexes. In addition, a correction was performed for the fraction of light absorbed when the CDx samples showed an absorption at the excitation wavelengths.[28]

Time-resolved fluorescence experiments were performed using a Ti:sapphire laser system and a Hamamatsu streak camera detection system.[29] The excitation wavelengths were set between 278 and 285 nm, and the polychrometer slit was set at 100 μm. The sample cell contained 3 mL of solution, and the iris between the cell and the first collection lens was set at a 5 mm diameter. The wavelength ranges on the polychrometer were set between 470−560 and 360−450 nm, and the total collection time ranges were 20 and 5 ns for fluorenone and xanthone, respectively. The binarization mode with a threshold level of 10 was used, and shading corrections within the Hamamatsu software were performed. The counts per cycle were kept below 0.05 for both the samples and instrument response function (IRF) acquisitions. The IRF was obtained by collecting the scattering of the laser light from a cell containing water. The number of acquisition cycles was set to obtain at least 10 000 counts between the wavelength ranges integrated (498−528 and 391−403 nm for fluorenone and xanthone, respectively). The raw data were transformed using a program written with Labview 4.0 (National Instruments) and were analyzed using a commercial PTI software. Since the binarization mode was employed, adequate fits were obtained with χ^2 values of 6. This high value is a consequence of the blurring of the signal over more than one pixel.[29] Samples were purged with nitrogen for 15 min before data collection.

Methods. Saturated aqueous fluorenone and xanthone solutions were prepared by stirring the solids with water for at least 48 h followed by filtration through Millipore filters (0.45 μm). CDx stock solutions containing 10−12 mM β-CDx or 30 mM α-CDx were prepared by dissolving the CDx in the saturated aqueous ketone solutions followed by stirring for at least 4 h. CDx solutions at lower concentrations were prepared by dilution with the saturated aqueous ketone solutions and were stirred for at least 10 h. CDx solutions in water in the absence of ketones were employed for the correction of absorbance, fluorescence, and ICD measurements.

Determination of Equilibrium Constants. The equilibrium constants (K_{eq}) for the ketone−CDx complexes were recovered from the analysis of the change in the ICD or fluorescence intensities with increasing CDx concentrations. The observed intensity change (ΔI) is given by eq 1[30] assuming a 1:n ($n = 1$ or 2) ketone/CDx stoichiometry, where for $n = 2$, no 1:1 complex is formed. In addition, the CDx concentration can be assumed to be constant, since it is present in an excess over the ketone concentration:

$$\Delta I = \frac{[\mathrm{K}]_T \Delta_x K_{eq} [\mathrm{CD}]^n}{1 + K_{eq}[\mathrm{CD}]^n} \quad (1)$$

where $[\mathrm{K}]_T$ is the total ketone concentration and Δ_x is related to the molar ellipticities of the complexed ketone in the case of ICD or the difference for the emission quantum yields of the free and complexed ketone in the case of the fluorescence experiments.

A linear relationship, frequently referred to as the Benesi−Hildebrand plot,[31] is obtained for the double-reciprocal plot of eq 1:

$$\frac{1}{\Delta I} = \frac{1}{[\mathrm{K}]_T \Delta_x} + \frac{1}{[\mathrm{K}]_T \Delta_x K_{eq} [\mathrm{CD}]^n} \quad (2)$$

The K_{eq} values were obtained from the nonlinear fit of the experimental data to eq 1 (Kaleidagraph software v. 3.0), since this plot properly weights the experimental data. However, eq 2 is very useful to check if the assumed stoichiometry is valid, since deviations from linearity are observed when the incorrect stoichiometry is assumed.

Alternatively, when a complex with 1:2 ketone/CDx stoichiometry is observed, the 1:1 complex can also be present at moderate CDx concentrations:

$$K + CD \overset{K_1}{\rightleftharpoons} KCD \tag{3}$$

$$KCD + CD \overset{K_2}{\rightleftharpoons} KCD_2 \tag{4}$$

The ΔI value is a function of the differences in molar ellipticities or differences of the fluorescence quantum yields for the ketone in solution and when incorporated into the 1:1 ($\Delta_x(1)$) and 1:2 ($\Delta_x(2)$) complexes.

$$\Delta I = \frac{[K]_T K_1 \Delta_x(1)[CD] + [K]_T K_1 K_2 \Delta_x(2)[CD]^2}{1 + K_1[CD] + K_1 K_2 [CD]^2} \tag{5}$$

Equation 5 is reduced to eq 6 when $\Delta_x(1)$ is equal to zero, which is the case when the fluorescence quantum yields are the same for the ketone in water and incorporated in a 1:1 complex:

$$\Delta I = \frac{[K]_T K_1 K_2 \Delta_x(2)[CD]^2}{1 + K_1[CD] + K_1 K_2 [CD]^2} \tag{6}$$

Calculation of Low-Energy Complex Structures. The computation of potential energies of CDx complex geometries is based on Allinger's MM3-92 force field applying a block diagonal matrix minimization method.[32] The fully minimized reference structures of α-CD and β-CD, derived from crystallographic data,[33] show energies of 61.5 and 71.3 kcal/mol, respectively. The potential energies of the guest molecules fluorenone and xanthone result in 14.2 and 5.8 kcal/mol, respectively. These reference structures are used in all the calculations described below.

Low-energy complex geometries are located by applying a dynamic Monte Carlo (DMC) routine[34] within the program package MultiMize.[35] Both, potential energies (calculated by the force field) and solvation effects (calculated by a continuum approximation assigning atomic solvation parameters σ_j to the solvent accessible molecular surface area A_j), are considered in a modified Metropolis criterion (eq 7). Details of the calculation are presented in ref 17

$$\Delta G_{solv} = \Delta G_{h-philic} + \Delta G_{h-phobic} = \left(\sum_j \Delta\sigma_j A_j\right)_{\sigma_j<0} + \left(\sum_j \Delta\sigma_j A_j\right)_{\sigma_j>0} \tag{7}$$

In an approximation the total free energy of solvation, ΔG_{solv}, is calculated as the sum over solvating hydrophilic surface areas, characterized by atomic solvation parameters $\sigma_j < 0$, and hydrophobic surface areas with the respective solvation parameters $\sigma_j > 0$, resulting in $\Delta G_{h-philic}$ and $\Delta G_{h-phobic}$, respectively. The atomic solvation parameter set σ_j of Wesson and Eisenberg in the adjustment of Sharp et al.[36] is used in our calculations. "Minimizing" the hydrophobic contact area (in our case solvent accessible carbon surfaces) and corresponding $\Delta G_{h-phobic}$ best resembles the hydrophobic effect crucial for CD complex formation.[17]

The start geometries for DMC runs are defined by a random relative orientation of the guest within a distance of 5 Å pointing toward the host cavity. In each DMC step this relative position is stochastically altered in the *x*, *y*, and *z* axes by a maximum of 0.5 Å, the guest is rotated by a maximum of 5°, and the individual glucose units within the host molecules are also rotated by a maximum of 5°. Each stochastically generated structure is fully minimized within the force field and accepted according to the modified Metropolis criterion.[17] The simulation temperature is kept constant at 300 K, and low-energy complex structures are obtained within 1000 DMC steps. Besides potential and solvation energies, the complexes are characterized by a host−guest distance defined by the distance between the center of mass of the guest and the mean position of the glycosidic oxygens of the macrocycle.

Calculation of the ICD Spectra. The ICD spectra, corresponding to the structures of lowest energy generated by the stochastic procedure described above, were calculated following the Kirkwood−Tinoco framework.[37] Out of the three mechanisms that generally describe the induction of rotatory power in a complex, i.e., the one-electron, the dipole−dipole, and the magnetic−electric interaction, the second appears to be the most important in this case. A particularly useful approximation is obtained by introducing, in Kirkwood's equations, the polarizability of the bonds of the chiral macrocycle in place of the original dipole−dipole interaction scheme.[37] Along this approximation, the pertinent expression of the rotatory strength for a transition $0 \rightarrow a$ is given by

$$R_{0a} = \pi \nu_a \mu_{0a}^2 \sum_j \frac{\nu_{0j}^2 (\alpha_{33} - \alpha_{11})_j (GF)_j}{c(\nu_{0j}^2 - \nu_a^2)} \tag{8}$$

$$(GF)_j = \frac{1}{r_j^3}\left[\mathbf{e}_{0a}\mathbf{e}_j - \frac{3(\mathbf{e}_{0a}\mathbf{r}_j)(\mathbf{e}_j\mathbf{r}_j)}{r_j^2}\right]\mathbf{e}_{0a} \times \mathbf{e}_j\mathbf{r}_j \tag{9}$$

where $\mathbf{e}_{0a}$ and $\mathbf{e}_j$ are unit vectors along the electric transition moment μ_{0a} and parallel to the *j*th bond, respectively, ν_{0j} and ν_a are frequencies of the electric transitions of host and guest, which are located at a distance r_j, and α_{11} and α_{33} represent bond polarizabilities at zero frequency parallel and perpendicular to the symmetry axis of the *j*th bond. In eq 8 the energies and electric moments were calculated using the CNDO/S program, with the Mataga−Nishimoto approximation for the Coulomb integrals and CI = 120 singly excited configurations. Being that the rotational strength is directly proportional to the factor expressed by eq 9, it turns out that the method is also quite sensitive to slight variations of the geometric setup. The rotational strengths calculated were inserted into a sum of Gaussian functions, which were appropriate in simulating the CDx spectrum in the region examined.[38]

The combined procedure described above (DMC + ICD) is selective enough to restrict the number of reliable low-energy structures; e.g., in a typical calculation with 1000 DMC steps, 200 structures are accepted for which the 10 structures with the lowest energy only 1 or 2 gave reasonable ICD spectra. For this reason, we can assume that the choice of one structure as shown in the figures below is a meaningful representation of the average position of the guest within the complex.

Results

Complexation of Xanthone. Fluorescence and ICD spectroscopy have been previously employed to characterize the complexes between xanthone and α-, β-, γ-, and hydroxypropyl-β-CDxs.[21,23] Binding is strongest with hydroxypropyl-β- (1800 ± 100 M^{-1}) followed by β- (1100 ± 200 M^{-1}), γ- (200 ± 30 M^{-1}), and α-CDx (50 ± 8 M^{-1}). These equilibrium constants were obtained from fits of the fluorescence or ICD data to eq

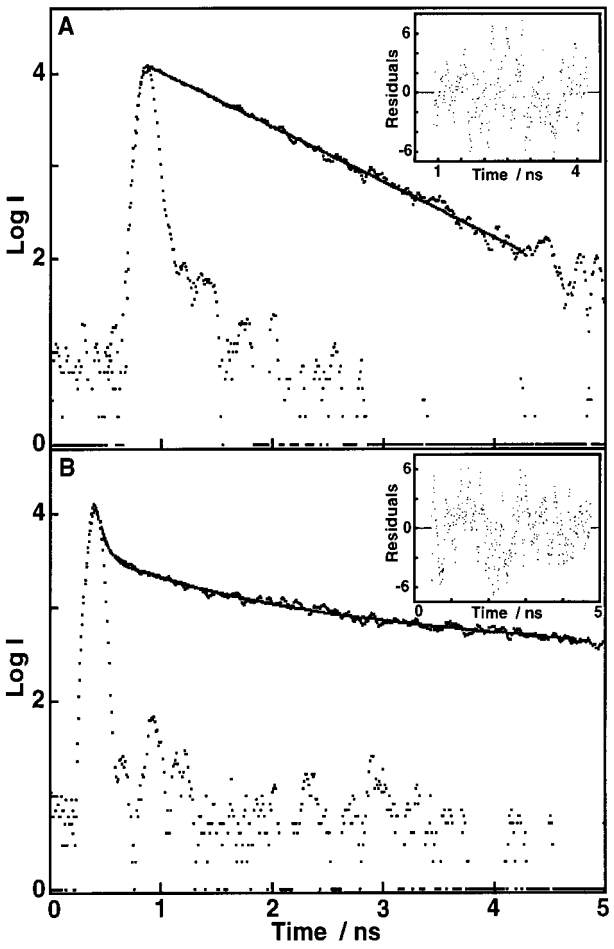

Figure 1. Time-resolved fluorescence decays of xanthone in the absence (A) and presence (B) of 8 mM β-CDx fitted to one exponential (A) and the sum of three exponentials (B). The residuals for the fits are shown in the insets.

1 for a 1:1 xanthone/CDx stoichiometry. This stoichiometry was confirmed by linear double-reciprocal plots.[21]

The complexation of xanthone with α- and β-CDx was further characterized in the present study by measuring the time-resolved fluorescence of xanthone in the absence and presence of CDxs. It was previously shown that xanthone fluorescence occurs in the subnanosecond time domain. Although complexation of xanthone to CDx leads to a change in the decay profile, no accurate measurements were possible with nanosecond single-photon counting.[21] The decay of xanthone in water is monoexponential with a lifetime of 750 ± 50 ps (Figure 1). In the presence of β-CDx (8 mM) the fluorescence decay is multiexponential and can be fitted to the sum of three exponentials with lifetimes of 50−80 ps, 600−800 ps, and 3−5 ns (Figure 1). The largest preexponential term (>0.80) is associated with the species that has a 50−80 ps lifetime, and it was assigned to the emission of xanthone in the 1:1 CDx complex. The species with a 600−800 ps lifetime and a preexponential factor of ca. 0.15 corresponds to the emission of xanthone in water. Both these species show time-resolved emission spectra with maxima between 390 and 400 nm, which is characteristic for xanthone fluorescence. The long-lived component is a minor species, since its preexponential factor is less than 5%. No defined spectrum is associated with this species, and it is also present when a solution containing only CDx is irradiated by the laser. It clearly corresponds to an artifact that is related to either background detection of irradiation or impurities in the CDx. This artifact is particularly noticeable when the fluorescence of compounds with low quantum yields, such as fluorenone or xanthone, is being measured. In the presence of 30 mM α-CDx the fluorescence decay of xanthone can be adequately fitted to a monoexponential decay with a lifetime close to that observed for xanthone in water, suggesting that xanthone is not very protected from the aqueous phase when it is complexed to α-CDx. In principle, a biexponential decay is also expected for xanthone in the presence of 30 mM α-CDx, since an appreciable amount of xanthone is bound to the CDx and a decrease of the steady-state fluorescence emission intensity is observed. However, the intensity only decreases to 80% of the value in the absence of CDx, which would lead to a ratio of lifetimes of 1.25. This difference is too small to be observable, and for this reason the decay is adequately fitted to a monoexponential decay.

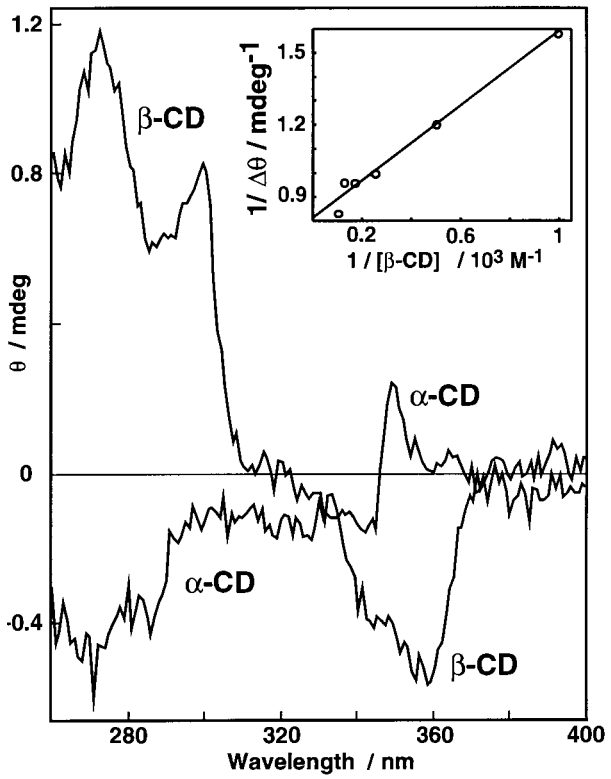

Figure 2. Xanthone ICD spectra in the presence of 8 mM β-CDx and 30 mM α-CDx. The inset shows the double-reciprocal plot for the variation of the xanthone ICD signal at 262 nm in the presence of different β-CDx concentrations.

The presence of α- or β-CDx leads to small blue shifts in the absorption spectra of xanthone without significantly changing the band shape. The ICD signals for xanthone complexed to α- and β-CDx have opposite signals in the long- and short-wavelength regions (Figure 2). In the case of β-CD, the values for the equilibrium constant using eq 1 for a 1:1 stoichiometry are 1000 ± 200 and 1200 ± 300 M^{-1} for measurements at 262 and 350 nm, respectively. These two wavelengths correspond to two different transitions in the ICD spectrum, and the recovered values for the equilibrium constants are the same as previously determined.[21,23] In addition, the double-reciprocal plots are linear (inset Figure 2), suggesting that the complex has a 1:1 stoichiometry.

The 1:1 complexes of xanthone with α- and β-CDx, as well as the 1:2 complexes with α-CDx, were calculated with DMC runs to gain insight into the structural features of the low-energy geometries. Xanthone is not tightly bound to α-CDx (Figure 3A). It is only attached to a part of the secondary hydroxyl rim side as attested by the relatively large host−guest distance of

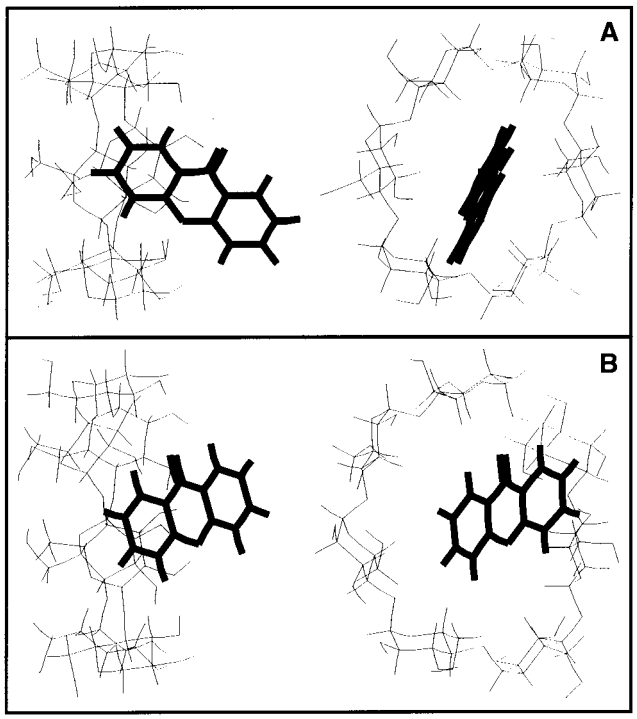

Figure 3. Calculated structures for the 1:1 complexes of xanthone with α-CDx (A) and β-CDx (B).

3.9 Å. The macrocycle shows the slight distortion that is also observed for the crystal structure of α-CDx. In addition, the guest molecule for the calculated structure of fluorenone and α-CDx is mostly exposed to the solvent. All the low-energy structures with a complexation energy of around −14 kcal/mol, defined as the energy difference between the sum of potential energies of the isolated CDx and xanthone and the energy of the complex, are of the geometry type shown in Figure 3, which also gives the correct ICD signal. Deeper penetration of the guest yields an energy increase of around 8 kcal/mol. No stable 1:2 complexes with α-CDx is found in DMC runs. A more stable 1:1 complex (−18.8 kcal/mol) is calculated for the interaction of xanthone with β-CDx with a host−guest distance of 2.6 Å, suggesting that xanthone penetrates deeper into the larger β-CDx cavity (Figure 3 B). Furthermore, the guest molecule is still significantly exposed to the solvent and xanthone is tilted in order to gain additional stabilization by interacting with a part of the secondary hydroxyl rim of the CDx. The structure of β-CDx in the complex shows significant deviations from the crystal structure, as generally found in β-CDx complexes.[17,39] The seven-membered ring is found to be highly flexible in solution and easily adapts its structure to steric constraints of the guest molecule.

The calculated ICD spectra for xanthone complexed to α- and β-CDx (Figure 4) show the specular behavior observed for the experimental spectra (Figure 2) with a negative low-energy band for β-CDx, a positive one for α-CDx, and a reversal in both cases in the short-wavelength region. The calculated energies appear overestimated especially for the low-lying π,π^* transitions, as frequently found with the present method for carbonyl compounds.[40,41] The relative intensities of the low- and high-energy bands are well reproduced by the calculations for the complex with β-CD, whereas in the case of α-CD the intensity of the short-wavelength band is overestimated. The calculated spectra show a fairly high consistency with the signs of the bands around the most stable energy minima calculated. A reversal of the sign is only observed for higher energy structures associated with larger xanthone−CDx distances.

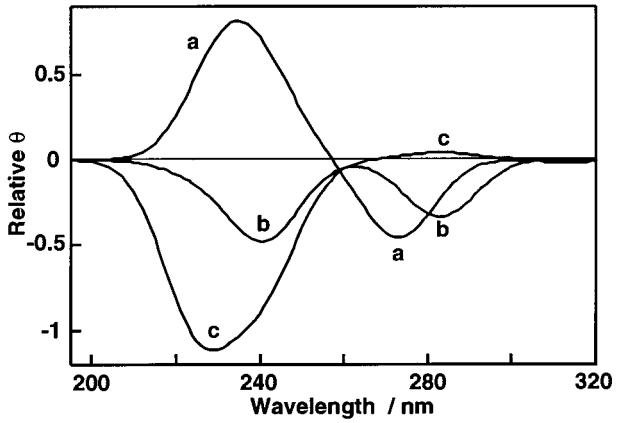

Figure 4. Calculated ICD spectra for xanthone complexed to β-CDx (a), two α-CDxs (b), and α-CDx (c).

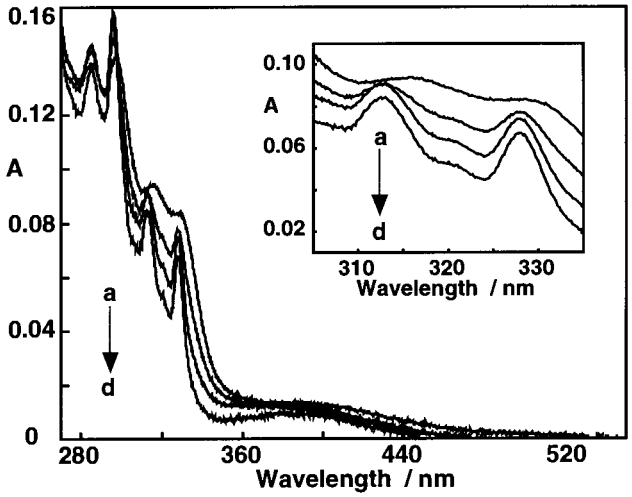

Figure 5. Corrected fluorenone absorption spectra in the presence of α-CDx at the following concentrations (mM): (a) 0; (b) 10; (c) 20; (d) 30. The inset shows an enlargement of the spectra between 290 and 340 nm.

Complexation of Fluorenone. Fluorenone was chosen as an alternative guest to xanthone because it is of a similar size, and both molecules have excited states that are close in energy but have different configurations in both the singlet and triplet manifold, leading to a complex photophysical behavior. In contrast to xanthone, where the behavior of the triplet absorption can be exploited to measure its complexation dynamics,[21−23,42] fluorenone was found to have a very low intersystem crossing quantum yield in water due to a significant increase of the internal conversion rate constant in hydroxylic solvents.[43−46] However, the complexation behavior for these two ketones is quite different.

A small enhancement is observed for the absorbance of fluorenone in the presence of β-CDx, suggesting that fluorenone is incorporated in the host molecule. This change is too small to be useful for the determination of the equilibrium constant between fluorenone and β-CDx. In contrast, in the presence of α-CDx a significant sharpening of the fluorenone absorption spectrum is observed at high CDx (≥10 mM) concentrations (Figure 5). No isosbestic point is detected, indicating that more than one type of complex is formed.

The fluorescence quantum yield and emission maxima of fluorenone are dependent on the solvent polarity, and the quantum yields are less than 0.04.[45−51] In nonprotic solvents the fluorescence lifetime and emission quantum yields increase with solvent polarity. However, in protic solvents the fluores-

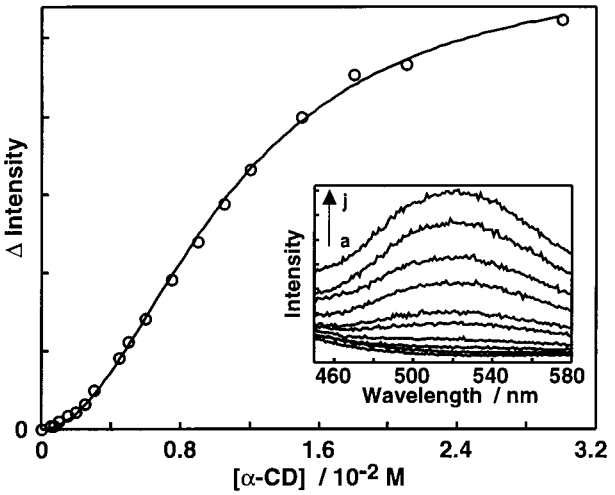

Figure 6. Nonlinear fit (eq 6) of the corrected fluorenone fluorescence intensities at 525 nm in the presence of various α-CDx concentrations. The inset shows the corrected fluorescence spectra of fluorenone in the presence of different α-CDx concentrations: (a) 0, (b) 1, (c) 2, (d) 3, (e) 5, (f) 6, (g) 9, (h) 12, (i) 18, and (j) 30 mM.

cence of fluorenone is quenched by hydrogen bonding with the solvent.[44−46] The fluorescence quantum yield for fluorenone in ethanol has been reported to be 1.5×10^{-3},[46] and we observed a weak emission in this alcohol. In contrast, no emission from fluorenone in water was detected for the same experimental conditions as employed for ethanol, which suggests that the fluorescence quantum yield in the aqueous solution is less than 1.5×10^{-4}.

In the presence of low concentrations of α-CDx (<3 mM) a very small increase is observed for the emission intensity above the baseline of the fluorimeter (Figure 6). However, at higher CDx concentrations (>5 mM) the emission increases markedly and has a maximum at 525 nm (inset Figure 6). On the basis of the α-CDx concentration dependence on the fluorescence intensity, the observed emission is assigned to the fluorenone in a 1:2 guest−host complex. The addition of *β*-CDx did lead to the detection of only a small enhancement of the fluorenone fluorescence, suggesting that fluorenone in this complex is fairly exposed to water.

The change in the fluorenone emission intensity with α-CDx concentration cannot be fitted to eq 1 assuming a 1:2 stoichiometry. Likewise, the double-reciprocal plot (eq 2), assuming the same stoichiometry, is not linear. These results indicate that the 1:1 complex has to be taken into account when fitting the fluorescence data. Since only a very small increase was observed for the fluorescence intensity at low α-CDx concentrations, we assumed that the emission quantum yields for fluorenone in water and in the 1:1 complex are the same. This assumption is also based on the fact that fluorenone is exposed to water in the 1:1 complex as indicated from the calculations of the complex structure (see below). The fit of the data to eq 6 yields several combinations of K_1 and K_2 values that lead to acceptable fits as defined by the difference of the calculated and experimental data points. The product K_1K_2 for the acceptable fits is $(9.3 \pm 0.6) \times 10^3$ M^{-2}. This product is fairly constant for all acceptable fits, but the individual equilibrium constants ($K_1 = 1-50$ M^{-1} and $K_2 = 8700-200$ M^{-1}) varied considerably, suggesting that the individual equilibrium constants cannot be determined from the fluorescence data. The same values were obtained for K_1K_2 when the intensities were measured at fixed wavelengths or for the integrated fluorescence areas.

Time-resolved fluorescence experiments were only performed for fluorenone in the presence of high α-CDx concentrations,

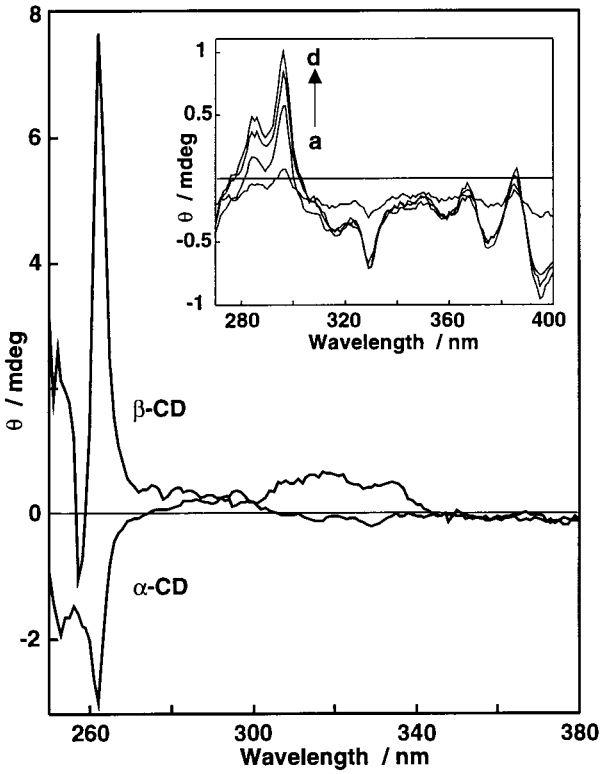

Figure 7. Fluorenone ICD spectra in the presence of 8 mM *β*-CDx and 30 mM α-CDx. The inset shows the ICD spectra of fluorenone in the presence of different concentrations of α-CDx: (a) 5, (b) 15, (c) 20, and (d) 30 mM.

since no appreciable fluorescence was observed at lower α-CDx concentrations. In the presence of 20−30 mM α-CDx, a biexponential decay was observed where the shorter component had a lifetime longer than 1.5 ns, suggesting that only one species of fluorenone was being detected. The longer component corresponds to an artifact similar to that observed for the time-resolved studies of xanthone with CDxs (see above).

The ICD spectra for fluorenone in the presence of α- and *β*-CDx show opposite signals for most of the spectral region investigated (Figure 7). In the case of *β*-CD, only positive signals are observed, whereas for α-CDx a more structured spectrum with negative and positive signals was measured (inset Figure 7). The change in the ICD intensity with increasing *β*-CD concentrations was fitted to eq 1 assuming a 1:1 stoichiometry, and the recovered value from four independent experiments for K_1 is (450 ± 50) M^{-1}. The double-reciprocal plots are linear, suggesting that the complexation stoichiometry is indeed 1:1.[52] In the case of α-CDx, the change in the ICD intensity is different for the band with a maximum at 296 nm than that at 330 nm (inset of Figure 7). The double-reciprocal plots for the changes at 296 and 330 nm fit reasonably well assuming a 1:1 and 1:2 stoichiometry, respectively. However, any attempts to obtain values for K_1 and K_2 failed, since very large errors were recovered.

The low-energy structure calculated from DMC runs for the 1:1 complex of fluorenone with α-CDx has the fluorenone interacting with the secondary hydroxyl rim without penetration of the cavity (Figure 8A). The host−guest distance is larger (4.9 Å) than observed for the complexation of xanthone. The low-energy structures always have the fluorenone attached to the rim, and deeper penetration leads to an energy increase of 5−10 kcal/mol. In contrast to xanthone, a 1:2 fluorenone/α-CDx complex was found in the DMC runs (Figure 9). In comparison, the guest is more deeply included in one host

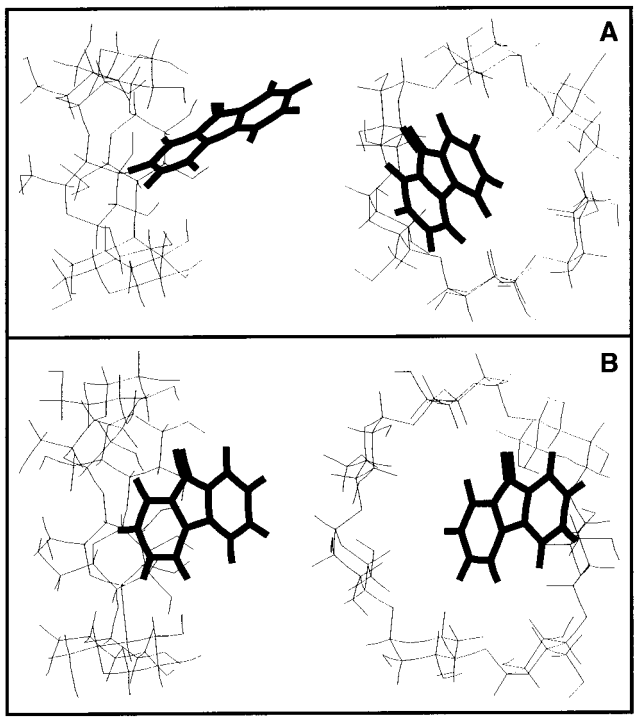

Figure 8. Calculated structures for the 1:1 complex of fluorenone with α-CDx (A) and *β*-CDx (B).

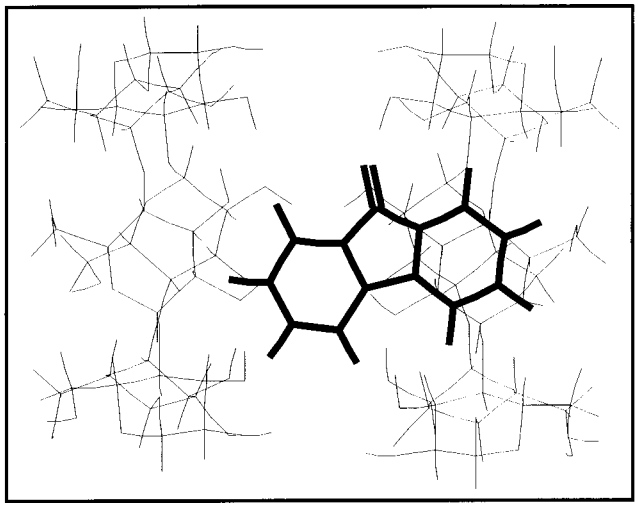

Figure 9. Calculated structure for the 1:2 complex of fluorenone with α-CDxs.

molecule but only attached to the other. The gain in complexation energy is ca. −28 kcal/mol compared to −12.8 kcal/mol calculated for the 1:1 complex. Besides the interaction between host and guest, the enhanced stability of the 1:2 complex is mainly based on the interaction of the CDx molecules forming various intermolecular hydrogen bonds between hydroxyl groups of the secondary CD rim.

The 1:1 complex of fluorenone with *β*-CDx shows a higher stabilization compared to the complexation with α-CDx (Figure 8B). The host−guest distance is smaller (2.7 Å), but the guest is also considerably tilted and preferentially attached to one side of the cone.

The ICD spectra of fluorenone in α- and *β*-CDx (Figure 7) show an almost specular behavior with a rather flat part corresponding to the first absorption system and a sharp positive (in *β*-CDx) and negative (in α-CDx) signal at 270 nm in the region. This behavior is fairly well reproduced by the calculated

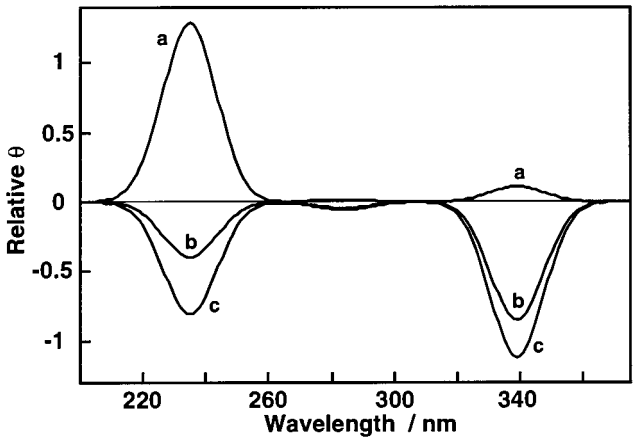

Figure 10. Calculated ICD spectra for fluorenone complexed to *β*-CDx (a), α-CDx (b), and two α-CDxs (c).

sequence of ICD signals for *β*-CDx (Figure 10), which gives rise to a totally positive spectrum, with the first signal calculated at 330 nm, the second, very weak, at 275 nm, and the largest one at 235 nm in correspondence to the most intense π,π^* experimental ICD band detected at 270 nm. Generally, the signals appear larger for the inclusion in *β*-CDx than in α-CDx, a feature consistent with a better included chromophore and a well defined 1:1 complex for the former case (see above). On the other hand, inclusion of fluorenone in α-CD results in a sequence of calculated negative signals along the entire CD spectrum. The calculation tends to overestimate the size of the first band, while the band at shorter wavelengths is calculated correctly (negative and less intense than in *β*-CDx). The effect of inclusion of fluorenone in two α-CDx results in a more stable complex, which reflects also in a more negative sequence of bands. The results for the calculated and experimental ICD spectra are not in complete agreement, reflecting the complexity of the fluorenone complexation to α-CDx (see below).

Discussion

Insights into the structural parameters of CDx complexes can be obtained by analyzing the predicted ICD spectra for optimized guest−CDx complexes obtained from molecular mechanics calculations and comparing these spectra to the experimental ones.[16−18,38] The method employed combines potential energy calculations with a force field, as well as free energies of solvation derived from a continuum approximation.[16,17,38] The contributions arising from solvation effects, which for CDx complexes are mainly due to hydrophobic interactions, are an important prerequisite in order to obtain correct complex geometries.[17] For example, the molecular motions for the loose complex of phenol included within the *β*-CDx cavity are restricted when solvent effects are included in the DMC calculations.[17,18] In contrast, for the bulkier 2,4,6-trimethylphenol a limited number of defined structures are achieved that position the guest at the rim of the CDx.[17,18] One important feature of this latter complex is the influence of the stability of the intramolecular hydrogen bonds on the secondary rim of *β*-CDx.[17] In addition, it was shown that when the guest molecules are larger than the CDx cavity, the formation of higher order complexes (e.g., 1:2 guest/CDx) is observed,[53] and this feature is reproduced by the DMC calculations.[16,38]

Complexation of Ketones to *β*-CDx. The largest equilibrium constants for xanthone and CDxs were observed for *β*-CDx followed by *γ*- and α-CDx,[21] suggesting that the best size complementarity is obtained with *β*-CDx. The cavity of α-CDx

is too small to efficiently complex xanthone. The same features were observed for fluorenone complexed to α- and β-CDx.

The xanthone fluorescence decay in the presence of β-CDx is not monoexponential. It is composed of a short-lived species with a lifetime of ca. 50−80 ps and a second component with lifetimes between 600 and 800 ps. The latter species corresponds to the decay of xanthone in water, for which a lifetime of 750 ps was measured. The short-lived component was assigned to xanthone complexed to β-CDx. These assignments are consistent with the decrease observed for the steady-state fluorescence intensity when xanthone is complexed to CDxs.[21] The behavior of the excited singlet decay for xanthone complexed to β-CDx parallels that observed for the incorporation of this ketone in anionic and cationic micelles, where a substantial shortening of the lifetime was observed for xanthone associated with the micellar environment.[54] The photophysics of xanthone is quite complex because several energy levels with either π,π^* or n,π^* configurations are close in energy in both the singlet and triplet manifolds. The intersystem crossing for xanthone was shown to depend on the solvent polarity,[55] and even in methanol or ethanol the buildup time for the triplet, which is directly related to the excited singlet decay, is shorter than 20 ps.[55,56] In this respect, water significantly alters the photophysics of xanthone, since the singlet lifetime is enhanced by over 1 order of magnitude compared to the decay in alcohols. Complexation of xanthone to β-CDx reduced the excited singlet lifetime from 750 ps to ca. 65 ps, suggesting that the ketone is somewhat protected from water. However, this lifetime value is still longer than that observed in alcohols, suggesting that the polarity sensed by the complexed xanthone is intermediate between that for alcohols and water. This result is consistent with the calculated structure of the complex where the ketone is attached to the rim of β-CDx and is not completely included in the cavity.

In the case of fluorenone, the complexation efficiency with β-CDx could only be determined from the ICD spectra, since the changes in its absorption spectra are small and since this ketone does fluoresce only weakly in the presence of β-CDx. The fluorescence quantum yield of fluorenone in hydroxyl solvents is very low.[43−46] For this reason, the lack of fluorescence when this ketone is complexed to β-CDx indicates that it is either somewhat exposed to water or its carbonyl group is hydrogen-bonded to the hydroxyl groups of the CDx rim.

The complexation of xanthone and fluorenone with β-CDx occurs with a 1:1 stoichiometry as attested by the linear double-reciprocal plots for the change of the ICD signals for both ketones with the change in CDx concentrations. The equilibrium constant between β-CDx and xanthone is higher (1100 ± 200 M^{-1}) than for fluorenone (450 ± 50 M^{-1}), indicating that for the former the complex is stabilized by about 0.5 kcal/mol compared to the latter. The calculations for the low-energy structures of both ketones with β-CD lead to very similar host−guest distances and complexation energies. The only difference observed was that xanthone is more axially aligned, and the calculated ICD spectra for this ketone are more sensitive to structural changes of the complex than observed for fluorenone, suggesting that for xanthone a more defined complex exists. This result is in line with the larger equilibrium constant measured for xanthone when compared to fluorenone, suggesting that the rigidity of the complex predicted from the calculations has direct bearing on the complexation efficiency of guest molecules to CDxs.

The ICD spectra calculated for the optimized structures of xanthone and fluorenone with β-CDx agree very well with the experimental spectra. In both cases, the ketones do not penetrate deeply into the CDx cavity. Deeper penetration leads to higher energies for the calculated structures, and the predicted ICD spectra deviate considerably from the experimental ones, especially in the case of fluorenone. In the aqueous phase, the ketones are hydrogen-bonded to water molecules, and deep inclusion into the CDx cavity would preclude any formation of hydrogen bonds, which is energetically unfavorable. Binding to the rim of the CDx cavity leads to minimization of the exposure of the hydrophobic surface of one aromatic ring to water without breaking all the hydrogen bonds. In this respect, the positions of xanthone and fluorenone within the complex represent a compromise between the energetically favorable shielding of the hydrophobic surfaces from water and the unfavorable breaking of hydrogen bonds. The photophysical studies agree very well with the fact that xanthone and fluorenone are included in β-CDx but are somewhat exposed to the aqueous phase (see above).

Complexation of Ketones to α-CDx. The binding of xanthone to α-CDx is much less efficient than for β-CD as attested by the much lower equilibrium constant (50 ± 8 M^{-1}).[21] In the complex with α-CDx, xanthone will be more exposed to the aqueous phase because of the smaller size of this cavity when compared to β-CDx. In principle, a nonexponential decay was expected for the xanthone fluorescence in the presence of α-CDx, since in the steady-state experiment its emission intensity is decreased in the presence of α-CDx. The observed monoexponential decay can be explained by an excited singlet lifetime for the complexed xanthone that is close to the lifetime in water. In this respect, a longer lifetime than observed for xanthone in β-CDx would be expected, since the guest is more exposed to water when associated with the smaller CDx.

The binding between fluorenone and α-CDx is more complex than the behavior observed for xanthone. At low α-CDx concentrations, the absorption spectrum of fluorenone only changes slightly. However, at higher concentrations (≥10 mM) the absorption spectrum of fluorenone sharpens significantly. Broad absorption spectra in the 300 nm region are observed for fluorenone in water or ethanol but not in acetonitrile or *tert*-butyl alcohol. The sharpening observed at high α-CDx concentrations indicates that fluorenone is fairly well protected from the interaction with water molecules. This result is consistent with the formation of a 1:2 fluorenone/α-CDx complex. In addition, the lack of an isosbestic point suggests that other complexes, such as the 1:1 complex, are also present.

The lag observed in the increase of the fluorescence intensity with α-CDx concentration is consistent with the formation of a 1:2 complex. The fluorenone fluorescence maximum is known to shift from 490 nm in toluene to 510 nm in acetonitrile[51] and 550 nm in ethanol.[44] The emission maximum for the fluorenone/α-CDx complex was observed at 525 nm, suggesting that the polarity sensed is less than that for ethanol. This result is also consistent with the assignment that fluorenone is in a fairly apolar environment. Furthermore, the lifetime in excess of 1.5 ns for the complex is longer than the lifetime for fluorenone in ethanol (0.8 ns).[46] Since the decay of fluorenone in hydroxylic solvents is accelerated due to hydrogen bonding, the longer lifetime in the presence of α-CDx indicates that fluorenone is not extensively hydrogen-bonded in the 1:2 complex. This fact is confirmed by the optimized structure calculated, where the guest's hydrogen-bonding functionality in the 1:2 complex is indeed mostly shielded from the bulk water. In addition, water molecules cannot be positioned between the two CDx units to

participate in hydrogen bonds with the guest, and hydrogen bonds between the guest and the host are geometrically unfavored.

The presence of more than one complex between fluorenone and α-CDx at high CDx concentrations is suggested by the lack of isosbestic points in the absorption spectra and the dependence of the change in the fluorescence and ICD intensities with increasing CDx concentrations. In both cases, the double-reciprocal plots are nonlinear when either a 1:1 or 1:2 complexation stoichiometry is assumed. The formation of the 1:2 complex is relatively efficient, since the lower limit for the K_2 value is around 200 M^{-1}.

The optimized structures for the 1:1 complexes of xanthone and fluorenone with α-CDx show that the ketones are more exposed to the aqueous phase than when they are complexed to β-CDx. This behavior is consistent with the photophysical data. In addition, the calculated ICD spectra for the optimized xanthone/α-CDx structures reproduce well the experimental spectra. In the case of fluorenone, the presence of the 1:1 and 1:2 complexes leads to a more complex behavior of the ICD spectra (see below). In contrast to the complexation of both ketones to β-CDx, the host−guest distances are very different for the 1:1 complex between xanthone or fluorenone with α-CDx. In both cases, there is less penetration of the ketones into the α-CDx cavity than observed for β-CDx, but xanthone is included further into α-CDx (3.9 Å host−guest distance) than fluorenone (4.9 Å). In addition, fluorenone is much more tilted than xanthone, suggesting that a more defined complex is formed for xanthone than for fluorenone as was also observed for the complexation of these ketones with β-CDx.

No evidence was obtained from the photophysical studies or the DMC calculations for a 1:2 complex between xanthone and α-CDx. In contrast, fluorenone does form a higher ordered complex. This difference could be related to the fact that in the 1:1 complex with fluorenone the guest is more exposed to water than in the case of xanthone, and this exposure provides an appropriate site for the binding of the second α-CDx molecule. DMC runs lead to a stable 1:2 complex in which fluorenone is more deeply included in one CDx molecule but is only attached to the second one. The increase in potential energy when the guest penetrates the CDx cavity is counteracted by a favorable interaction when the CDx molecules are in proximity. The deeper penetration of fluorenone is attested by the shortening of the host−guest distance by about 2 Å in the 1:2 complex when compared to the 1:1 complex, suggesting that association of the second CDx forces a deeper penetration of the guest into one cavity so that the hydroxyl groups at the rim of the CDxs can interact. Fluorenone appears sufficiently shielded from the aqueous phase to experience a hydrophobic environment, as revealed by the fluorescence and ICD features.

The experimental ICD spectrum for fluorenone in the presence of α-CDx shows more features than predicted from the calculated spectrum. The calculated spectra for the 1:1 and 1:2 complexes of fluorenone in α-CDx lead to a sequence of negative bands. Although this result is in agreement with the experimental results for the short-wavelength band, the ICD signals appearing in the first spectral zone (inset Figure 7) and its variation with CDx concentration do not seem easily explainable in terms of simple host−guest interactions. Inspection of the inset in Figure 7 in the range 320−400 nm shows a sequence of sigmoidal signs that can have two different explanations. The first explanation points to the interaction of two chromophores, with generation of sigmoidal signals of excitonic type, indicating the presence of higher order complexes with 2:2 stoichiometry. Examples of this kind of multiple interaction have been recently described for the complexes of several chromophores included in cyclodextrins.[57,58] However, no evidence of a 2:2 complex was observed in the absorption or fluorescence experiments. An alternative explanation is that the ICD spectrum in this region, where the electronic signal is quite low, is dominated by vibronic interactions between a low-lying $n\pi^*$ and upper states of $\pi\pi^*$ nature. The appearance of a well-resolved sequence of positive and negative signals in this region can, in principle, be reconciled with the formation of a more rigid complex, e.g., of 1:2 type such as that shown in Figure 9. Recently, there has been an increasing amount of evidence that multiple complexation of this type modifies the spectral features, especially by narrowing the bands and influencing the photophysical behavior of the included guest.[59] By comparison with the band half-width detected in apolar hydrocarbon solutions, this effect was interpreted to be due to the nonpolar character of the CDx cavity experienced by the chromophore. On the other hand, the dependence of the CDx signal in the same spectral zone for inclusion of fluorenone in β-CDx shows a monotonic increase of positive intensity without the appearance of bands of different sign, indicating the absence of multiple interactions in this case and a well-defined 1:1 complex.

In conclusion, the theoretical calculations combined with the photophysical studies provide detailed information on the structure of the complexes between xanthone or fluorenone to CDxs. The structure of xanthone as well as fluorenone complexation with β-CDx does not lead to deep penetration of the ketones into the CDx cavity. The binding to the rim of the β-CDx could be one of the features responsible for the faster exit of triplet xanthone from the CDx cavity when compared to other guest molecules. The optimized structures for the ketone complexes with β- as well as α-CDx indicate that more defined complexes are formed with xanthone than with fluorenone. In addition, the formation of a higher order complex is only observed for α-CDx and fluorenone, which may be related to the degree of exposure of the guest to the aqueous phase in the 1:1 complex. These subtle differences in the complexation of the ketones are well reproduced by the theoretical studies showing that the methodology employed can yield useful and detailed information on the structure of host−guest complexes involving CDxs.

Acknowledgment. C.B. thanks the Natural Science and Engineering Research Council of Canada (NSERC), and B.M. thanks the Austrian Academy of Sciences within APART (Austrian Program for Advanced Research and Technology) for support of their research programs. R.S.M. thanks NSERC and the University of Victoria for graduate scholarships, and T.C.B. thanks the Conselho Nacional de Desenvolvimento Científico e Tecnológico, CNPq (Brazil) for a postdoctoral fellowship. The authors at Victoria thank J. Ausio (Department of Biochemistry and Microbiology) for the use of the CD spectrometer, L. Netter for support in software development for data analysis of the picosecond fluorescence system, and Cerestar for their kind gift of the cyclodextrin samples.

Supporting Information Available: A description of the picosecond fluorescence system and a figure for the nonlinear fit of the fluorenone ICD signal in the presence of β-CD are provided (5 pages). Ordering information is given on any current masthead page.

References and Notes

(1) Saenger, W. *Angew. Chem., Int. Ed. Engl.* **1980**, *19*, 344.
(2) Tabushi, I. *Acc. Chem. Res.* **1982**, *15*, 66.
(3) Szejtli, J. In *Cyclodextrins*; Szejtli, J., Osa, T., Eds.; Elsevier Science Ltd.: New York, 1996; Vol. 3, p 5.
(4) Jicsinszky, L.; Fenyvesi, E.; Hashimoto, H.; Ueno, A. In *Cyclodextrins*; Szejtli, J., Osa, T., Eds.; Elsevier Science Ltd.: New York, 1996; Vol. 3, p 57.
(5) Li, S.; Purdy, W. C. *Chem. Rev.* **1992**, *92*, 1457.
(6) Demarco, P. V.; Thakkar, A. L. *Chem. Commun.* **1970**, 2.
(7) Lipkowitz, K. B.; Raghothama, S.; Yang, J. *J. Am. Chem. Soc.* **1992**, *114*, 1554.
(8) McAlpine, S. R.; Garcia-Garibay, M. A. *J. Org. Chem.* **1996**, *61*, 8307.
(9) Muñoz de la Peña, A.; Ndou, T. T.; Zung, J. B.; Greene, K. L.; Live, D. H.; Warner, I. M. *J. Am. Chem. Soc.* **1991**, *113*, 1572.
(10) Schneider, H.-J.; Blater, T.; Simova, S. *J. Am. Chem. Soc.* **1991**, *113*, 1996.
(11) Harata, K.; Uedaira, H. *Bull. Chem. Soc. Jpn.* **1975**, *48*, 375.
(12) Kodaka, M. *J. Phys. Chem.* **1991**, *95*, 2110.
(13) Kodaka, M. *J. Am. Chem. Soc.* **1993**, *115*, 3702.
(14) Kamiya, M.; Mitsuhashi, S.; Makino, M.; Yoshioka, H. *J. Phys. Chem.* **1992**, *96*, 95.
(15) Marconi, G.; Monti, S.; Mayer, B.; Köhler, G. *J. Phys. Chem.* **1995**, *99*, 3943.
(16) Grabner, G.; Monti, S.; Marconi, G.; Mayer, B.; Klein, C. T.; Köhler, G. *J. Phys. Chem.* **1996**, *100*, 20068.
(17) Mayer, B.; Marconi, G.; Klein, C.; Köhler, G.; Wolschann, P. *J. Incl. Phenom. Mol. Recognit. Chem.* **1997**, *29*, 79.
(18) Marconi, G.; Mayer, B. *Pure Appl. Chem.* **1997**, *69*, 779.
(19) Connors, K. A. *J. Pharm. Sci.* **1995**, *84*, 843.
(20) Kleinman, M. H.; Bohne, C. In *Molecular and Supramolecular Photochemistry*; Ramamurthy, V., Schanze, K. S., Eds.; Marcel Dekker Inc.: New York, 1997; Vol. 1, p 391.
(21) Barra, M.; Bohne, C.; Scaiano, J. C. *J. Am. Chem. Soc.* **1990**, *112*, 8075.
(22) Barra, M. *Supramol. Chem.* **1997**, *8*, 263.
(23) Liao, Y.; Frank, J.; Holzwarth, J. F.; Bohne, C. *J. Chem. Soc., Chem. Commun.* **1995**, 199.
(24) Hashimoto, S.; Thomas, J. K. *J. Am. Chem. Soc.* **1985**, *107*, 4655.
(25) Turro, N. J.; Okubo, T.; Chung, C.-J. *J. Am. Chem. Soc.* **1982**, *104*, 1789.
(26) Turro, N. J.; Bolt, J. D.; Kuroda, Y.; Tabushi, I. *Photochem. Photobiol.* **1982**, *35*, 69.
(27) Barros, T. C.; Stefaniak, K.; Holzwarth, J. F.; Bohne, C. *J. Phys. Chem. A* **1998**, *102*, 5639.
(28) Yang, H.; Bohne, C. *J. Photochem. Photobiol. A* **1995**, *86*, 209.
(29) A detailed description of the picosecond fluorescence system is provided in the Supporting Information.
(30) Connors, K. A. *Binding Constants—The Measurement of Molecular Complex Stability*; John Wiley & Sons: New York, 1987.
(31) Benesi, H. A.; Hildebrand, J. H. *J. Am. Chem. Soc.* **1949**, *71*, 2703.
(32) Allinger, N. L.; Yuh, Y. H.; Lee, J. H. *J. Am. Chem. Soc.* **1989**, *111*, 8551.
(33) Betzel, C.; Saeger, W.; Hingerty, B. E.; Brown, G. M. *J. Am. Chem. Soc.* **1984**, *106*, 7545.
(34) Metropolis, N.; Rosenbluth, A. W.; Rosenbluth, M. B.; Teller, A. H. *J. Chem. Phys.* **1953**, *21*, 1087.
(35) Mayer, B. Program Package MultiMize, University of Vienna, Austria, 1997.
(36) Wesson, L.; Eisenberg, D. *Protein Sci.* **1992**, *1*, 227.
(37) Tinoco, I., Jr. *Adv. Chem. Phys.* **1962**, *4*, 113.
(38) Marconi, G.; Mayer, B.; Klein, C. T.; Köhler, G. *Chem. Phys. Lett.* **1996**, *260*, 589.
(39) Mayer, B.; Köhler, G. *J. Mol. Struct.: THEOCHEM* **1996**, *363*, 217.
(40) Jacques, P.; Faure, J.; Chalvet, O.; Jaffe, H. H. *J. Phys. Chem.* **1981**, *85*, 473.
(41) Kuboyama, A.; Kozima, Y.; Maeda, J. *Bull. Chem. Soc. Jpn.* **1982**, *55*, 3635.
(42) Liao, Y.; Bohne, C. *J. Phys. Chem.* **1996**, *100*, 734.
(43) Huggenberger, V.; Labhart, H. *Helv. Chim. Acta* **1978**, *61*, 250.
(44) Fujii, T.; Sano, M.; Mishima, S.; Hiratsuka, H. *Bull. Chem. Soc. Jpn.* **1996**, *69*, 1833.
(45) Biczók, L.; Bérces, T.; Linschitz, H. *J. Am. Chem. Soc.* **1997**, *119*, 11071.
(46) Biczóc, L.; Jicsinszky, L.; Linschitz, H. *J. Incl. Phenom. Mol. Recognit. Chem.* **1994**, *18*, 237.
(47) Singer, L. A. *Tetrahedron Lett.* **1969**, 923.
(48) Andrews, L. J.; Deroulede, A.; Linschitz, H. *J. Phys. Chem.* **1978**, *82*, 2304.
(49) Biczók, L.; Bérces, T. *J. Phys. Chem.* **1988**, *92*, 3842.
(50) Biczók, L.; Bérces, T.; Márta, F. *J. Phys. Chem.* **1993**, *97*, 8895.
(51) Murphy, R. S.; Moorlag, C. P.; Green, W. H.; Bohne, C. *J. Photochem. Photobiol. A* **1997**, *110*, 123.
(52) A figure showing the changes in the ICD intensity vs [β-CD] and the corresponding double-reciprocal plot is shown in the Supporting Information.
(53) Nigam, S.; Durocher, G. *J. Phys. Chem.* **1995**, *100*, 7135.
(54) Mohtat, N.; Cozens, F. L.; Scaiano, J. C. *J. Phys. Chem. B* **1998**, *102*, 7557.
(55) Cavaleri, J. J.; Prater, K.; Bowman, R. M. *Chem. Phys. Lett.* **1996**, *259*, 495.
(56) Damschen, D. E.; Merritt, C. D.; Perry, D. L.; Scott, G. W.; Talley, L. D. *J. Phys. Chem.* **1978**, *82*, 2268.
(57) Tamagaki, S.; Fukuda, K.; Maeda, H.; Mimura, N.; Tagaki, W. *J. Chem. Soc., Perkin Trans. 2* **1995**, 389.
(58) Marconi, G.; Mayer, B.; Monti, S.; Bortolus, P. To be published.
(59) Grabner, G.; Mayer, B.; Köhler, G. Presented at the XVIth IUPAC Symposium on Photochemistry, Helsinki, 1996; Book of Abstracts, 241.